



Ignition, Liftoff, and Extinction of Gaseous Diffusion Flames

Amable Liñán,¹ Marcos Vera,² and Antonio L. Sánchez²

¹Departamento de Motopropulsión y Termodinámica, Escuela Técnica Superior de Ingenieros Aeronáuticos, 28040 Madrid, Spain

²Departamento de Ingeniería Térmica y de Fluidos, Universidad Carlos III de Madrid, 28911 Leganés, Spain; email: asanchez@ing.uc3m.es

Annu. Rev. Fluid Mech. 2015. 47:293–314

The *Annual Review of Fluid Mechanics* is online at fluid.annualreviews.org

This article's doi:
10.1146/annurev-fluid-010814-014711

Copyright © 2015 by Annual Reviews.
All rights reserved

Keywords

triple flames, lifted flames, flame blow-off, strain-induced extinction, vortex-flame interactions

Abstract

This review uses as a vehicular example the jet-flame configuration to examine some phenomena that emerge in nonpremixed gaseous combustion as a result of the interaction between the temperature-sensitive chemical reaction, typical of combustion, and the convective and diffusive transport. These include diffusion-controlled flames, edge flames and their role in flame attachment, triple flames and their role as ignition fronts, and strain-induced extinction, including flame-vortex interactions. The aim is to give an overall view of the fluid dynamics of nonpremixed combustion and to review the most relevant contributions.

1. INTRODUCTION

The gas-phase combustion reactions between the oxygen of the air and, mainly, hydrocarbon fuels are characterized by their large exothermicity, leading to temperatures exceeding 2,000 K, and a very strong dependence of the overall reaction rate with temperature. Thus, at ambient temperature, the fuel can be partially mixed with air, even in gaseous form, with a negligible effect of the reaction, which will only take place after locally raising the temperature by an external energy source. When the energy deposited is small, of the order of a fraction of 1 mJ, the reaction can extend to the fuel-air mixture by a combustion front, self-propagating with a velocity of the order of 1 m/s. This premixed flame front, with a thickness of the order of 0.1 mm, separates the upstream chemically frozen reactant mixture from a downstream region in chemical equilibrium; the reaction occurs on its hot, downstream side, preceded by a layer in which the initially chemically frozen mixture is heated by conduction.

In many combustion processes, the fuel and oxygen are initially separated. After ignition, we find that in regions of high temperature, in which the reaction time is very short, the reactants coexist only, with small concentrations, in thin reaction layers, first termed “diffusion flames” by Burke & Schumann (1928). In these flames, the fuel and oxygen, after arriving from opposite sides, are completely consumed by the reaction while crossing the flame by diffusion. Liquid fuels must first be vaporized before burning in a gaseous diffusion flame, and this is also the case for the volatiles generated by solid fuels.

Diffusion flames are found in fireplaces as well as in wildland and urban fires. They are ubiquitous in engineering systems for propulsion and energy production, including diesel engines, gas turbines, rocket engines, and power-plant furnaces, and also in heating devices for domestic applications and in the process industry. Diffusion flames have also played a central role in the history of humankind, with the earliest applications involving the burning of wood for heating, illumination, cooking, and use as a dissuasive means against insects and ferocious beasts. Humans soon mastered the rudiments of ignition, initially starting a fire with a local increase of temperature by friction. They learned that they could enhance the burning rate by blowing and could promote flame spread from a locally ignited tinder and also that excessive blowing leads to flame extinction. This review addresses these processes of ignition, propagation, and extinction of diffusion flames.

A candle flame is an illustrative example of the broad variety of rich physicochemical phenomena that are present in nonpremixed combustion. As explained by Faraday (1861), the melted paraffin creeps up the cotton wick by capillary action and then vaporizes, at a rate controlled by heat conduction from the flame. As occurs in gaseous jet diffusion flames, the fuel vapor is transported by diffusion and convection toward the thin layer, or diffusion flame, in which it reacts with the oxygen that arrives, also by convection and diffusion, from the surrounding air. The buoyancy-induced motion in the candle flame, with characteristic velocities that scale with the free rise velocity, $\sqrt{gL_c}$, of the hot gases, with values of order 30 cm/s for flames with length $L_c \sim 3$ cm, enhances the air entrained by the flame and is also responsible for its slender appearance. The associated residence time, scaled with $L_c/\sqrt{gL_c} \sim 100$ ms, is much larger than the characteristic time, of the order of 1 ms, of fuel oxidation at the flame temperature. As a result, the overall structure of the candle flame is largely independent of the rate of this fast reaction; the flame appears as a thin layer in which the oxygen and fuel are completely consumed after arriving by diffusion in stoichiometric proportions. The thin reaction layer acts as a sink for the fuel vapor and oxygen, and a source for the heat released by the reaction and for the main reaction products, namely CO_2 and H_2O , which diffuse outside the flame, forming a hot envelope of products and air, and also inside the flame, heating and mixing with the fuel. The rate of fuel-vapor oxidation plays a dominant role in determining the location and structure of the premixed flame found

at the bottom of the candle flame, bounding the nonuniform mixture of air and fuel vapor that exists there as a result of the direct vaporization of the pool of liquid paraffin. This is melted by the heat arriving by radiation and conduction from the flame. Light from the micrometer-size soot particles, with a mass fraction measured in parts per million, gives the flame its characteristic yellow color, with the outer boundary of the yellow region defining the location of the diffusion flame in which the carbonaceous soot particles are oxidized. The rich underlying physics of the problem explains why, more than 150 years after Faraday (1861), the candle flame continues to be subject to current research (Sunderland et al. 2011).

An early review by Williams (1971) pointed out the role played by the high sensitivity with temperature of the combustion reactions in the existence of different nonpremixed combustion phenomena, including ignition, extinction, and triple flames (in addition to its central role in connection with premixed combustion fronts, namely detonations and deflagrations). We examine these finite-rate-kinetics aspects of nonpremixed flames below, after addressing the limit of diffusion-controlled combustion. Although in a number of nonpremixed combustion systems the fuel is introduced in the combustor as a liquid or a pulverized solid, we focus on gaseous combustion processes (see, e.g., Sirignano 2010 and Sánchez et al. 2015 for recent accounts of fluid mechanic aspects of spray vaporization and combustion). Whereas the present article deals with the general flame structure, including some unsteady effects, it does not address specific aspects of flame instability (Matalon 2007) or its control (Dowling & Morgans 2005).

In realistic applications, the Reynolds number is sufficiently large that the prevailing flow is turbulent. Detailed information on different aspects of nonpremixed turbulent flames is available in general monographs (Libby & Williams 1994, Peters 2000) and review articles (Bilger 1988, Bilger et al. 2005), including their numerical modeling (Veynante & Vervisch 2002) by direct numerical simulation (Vervisch & Poinso 1998) and by large eddy simulation (Pitsch 2006), as well as the structure of strained flamelets and their role in the extinction of diffusion flames (Peters 1984, Williams 2000). The topic of turbulent mixing, the rate-controlling mechanism in the limit of infinitely fast chemistry, has also been subject to a specific review (Dimotakis 2005). The present article, although not focused on turbulent combustion, appropriately acknowledges its importance in the discussion.

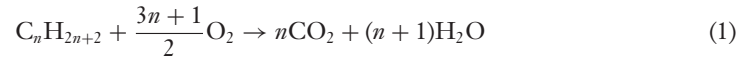
2. BASIC CONSIDERATIONS PERTAINING TO DIFFUSION-CONTROLLED COMBUSTION

We begin by presenting some fundamental aspects of diffusion flames, including the thermochemical parameters that ultimately determine the flame position and flame temperature when the irreversible chemical reaction is fast, a limit to be addressed in this section, after introducing the conservation equations.

2.1. Relevant Thermochemical Parameters

The oxidation of typical gaseous hydrocarbons involves hundreds of elementary chemical reactions among dozens of short-lived intermediate chemical species. Detailed kinetic schemes containing the needed elementary reactions, resulting from direct molecular collisions, and their associated rate constants are now well established for a few simple fuels, including hydrogen (Sánchez & Williams 2014) and some hydrocarbons (Miller et al. 2005, Simmie 2003). For many purposes, however, a simpler chemistry description suffices to investigate many aspects of combustion flows. For the discussion that follows, focused on the fluid mechanic aspects of nonpremixed combustion,

we adopt the overall reaction



as a representation of the underlying stoichiometry for the oxidation of a given saturated hydrocarbon of the general formula $\text{C}_n\text{H}_{2n+2}$. According to Equation 1, the unit mass of fuel reacts with a mass $s = 8(3n+1)/(7n+1)$ of oxygen to give a mass $s_{\text{CO}_2} = 22n/(7n+1)$ and $s_{\text{H}_2\text{O}} = 9(n+1)/(7n+1)$ of CO_2 and H_2O , respectively, releasing in the process an amount of energy given by $q = \frac{1}{2}(b_{\text{C}_n\text{H}_{2n+2}}^\circ - nb_{\text{CO}_2}^\circ - (n+1)b_{\text{H}_2\text{O}}^\circ)/(7n+1)$, where b_i° represents the enthalpy of formation per mole of species i . The resulting values of these parameters differ only by a small amount for hydrocarbons that share the same molecular structure, a characteristic that explains why their combustion properties are also very similar [e.g., $s = (4, 3.64, 3.48)$ and $q = (50.15, 46.46, 44.56)$ kJ/g for methane, propane, and dodecane, respectively].

In diffusion-controlled combustion systems, the streams that provide the air and the fuel are different. Below we use $Y_{\text{O}_2,A} \simeq 0.232$ and Y_{F0} to denote the mass fractions of oxygen and fuel in their respective feed streams, the latter taking values $Y_{F0} < 1$ in systems with fuel-feed dilution, which is often considered in experiments and numerical computations. These mass fractions can be used to calculate $S = sY_{F0}/Y_{\text{O}_2,A}$, the mass of air that one needs to mix with the unit mass of the gaseous fuel stream to generate a stoichiometric mixture. Adiabatic combustion of the resulting mixture at constant pressure would produce a final temperature T_S , given by

$$T_S - T_A = \frac{T_0 - T_A}{1 + S} + \frac{qY_{F0}}{c_p(1 + S)}, \quad (2)$$

if, for simplicity in the description, we approximate the specific heat c_p by a constant value. Here, T_A and T_0 denote the temperatures of the air and fuel streams, respectively. Two fundamental thermochemical parameters play an important role in nonpremixed combustion (see below), namely,

$$S = \frac{sY_{F0}}{Y_{\text{O}_2,A}} \quad \text{and} \quad \gamma = \frac{qY_{F0}}{c_p T_A(1 + S)}, \quad (3)$$

where the second parameter represents the dimensionless adiabatic combustion temperature increment due to chemical reaction. Typical values for S and γ in a hydrocarbon-air flame with undiluted fuel feed (i.e., $Y_{F0} = 1$) initially at normal ambient temperature are $S_u = s/Y_{\text{O}_2,A} \simeq 15$ and $\gamma \simeq 6.5$, the latter corresponding to a peak temperature, $T_S \simeq 2,300$ K.

As explained below, in nonpremixed flames the burning rate is diffusion controlled when the overall reaction given in Equation 1 is sufficiently fast so that its chemical kinetic rate becomes inconsequential. This rate is, however, important in diffusion-flame extinction processes and also for the propagation of premixed flame fronts, involved, for instance, in the ignition, liftoff, and attachment of diffusion flames. For the following discussion, we consider the simple irreversible Arrhenius rate expression

$$\omega = B e^{-E/(RT)} \left(\frac{\rho Y_F}{M_F} \right) \left(\frac{\rho Y_{\text{O}_2}}{M_{\text{O}_2}} \right) \quad (4)$$

for the moles of fuel consumed per unit volume per unit time, which is a function of the temperature T and of the reactant molar concentrations $\rho Y_F/M_F$ and $\rho Y_{\text{O}_2}/M_{\text{O}_2}$. Here, R and ρ denote the universal gas constant and the gas density, and Y_F and Y_{O_2} are the mass fractions and M_F and M_{O_2} the molecular masses of the fuel and oxygen, respectively. The rate parameters include the pre-exponential factor B and the activation energy E , which can be selected to reproduce the main combustion characteristics of a given hydrocarbon (e.g., the variation with composition of the propagation velocity of a steady, planar premixed flame) (Westbrook & Dryer 1981). This

propagation velocity is known to reach its maximum value $S_L \simeq 40$ cm/s when the mixture is stoichiometric (or slightly rich) and to decay rapidly for either leaner or richer conditions.

2.2. Conservation Equations

The conservation equations are the Navier-Stokes (NS) equations of mass, momentum, and energy supplemented with conservation equations for the different chemical species (Williams 1985). For the overall reaction given in Equation 1, the associated reactants and energy conservation equations reduce to

$$\frac{\partial}{\partial t}(\rho \hat{Y}_F) + \nabla \cdot \left(\rho \mathbf{v} \hat{Y}_F - \frac{\rho D_T}{L_F} \nabla \hat{Y}_F \right) = -\rho \hat{B} e^{-E/(RT)} \hat{Y}_F \hat{Y}_O, \quad (5)$$

$$\frac{\partial}{\partial t}(\rho \hat{Y}_O) + \nabla \cdot (\rho v \hat{Y}_O - \rho D_T \nabla \hat{Y}_O) = -S \rho \hat{B} e^{-E/(RT)} \hat{Y}_F \hat{Y}_O, \quad (6)$$

$$\frac{\partial}{\partial t} \left(\rho \frac{T}{T_A} \right) + \nabla \cdot \left(\rho \mathbf{v} \frac{T}{T_A} - \rho D_T \nabla \frac{T}{T_A} \right) = \gamma(1 + S) \rho \hat{B} e^{-E/(RT)} \hat{Y}_F \hat{Y}_O - \frac{\nabla \cdot \mathbf{q}_R}{c_p T_A}, \quad (7)$$

where \mathbf{v} is the gas velocity, D_T is the thermal diffusivity of the gas mixture, and $\hat{Y}_F = Y_F/Y_{F0}$ and $\hat{Y}_O = Y_{O_2}/Y_{O_2,A}$ are conveniently normalized reactant mass fractions, associated with a frequency factor $\hat{B} = (\rho Y_{O_2,A} B)/(M_F M_{O_2})$. For the conditions found in most combustion systems, the prevailing Mach number is small, so the kinetic energy of the gas and the viscous dissipation can be neglected, along with the spatial pressure variations in writing the energy equation (Equation 7). Temporal pressure variations, which are also omitted in Equation 7, must be retained in applications of combustion in confined chambers (e.g., in reciprocating engines) (Liñán & Williams 1993, 1995). The above equations must be complemented with similar equations for Y_{CO_2} and Y_{H_2O} and also with the well-known overall conservation equations for mass and momentum. Because radiative heat transfer is often nonnegligible (e.g., approximately 20% of the energy released in a typical domestic fireplace is transferred by radiation to the interior of the room), its effect has been retained in writing Equation 7, where \mathbf{q}_R represents the radiative heat flux.

To facilitate the following discussion, we have introduced a number of simplifications in the above equations. For instance, the energy equation (Equation 7) is written explicitly in terms of the temperature by neglecting differences in specific heat at constant pressure from the mean value c_p , as done above when computing the adiabatic flame temperature (Equation 2). In addition, a simple Fickian description has been adopted to write the diffusion velocities of the reactants. Because air is used as an oxidizer in most applications, molecular nitrogen becomes the dominant component of the gas mixture, with the result that the diffusivities of the reactants can be approximated by their binary diffusivities through N_2 . This approximation is even more accurate for systems with N_2 dilution of the fuel stream. The resulting diffusivity of oxygen is sufficiently close to D_T for the approximation $D_{O_2} = D_T$ to be adopted in writing Equation 6. In contrast, most hydrocarbon molecules are large, and their diffusivities D_F , although of the order of D_T , are smaller, so a Lewis number $L_F = D_T/D_F > 1$ must be considered in general in Equation 5, the approximation $L_F = 1$ being reasonably accurate only for methane, whereas $L_F \simeq 0.3$ for H_2 .

Equations 5–7 must be integrated with the appropriate initial and boundary conditions. For instance, one should use $\hat{Y}_F - 1 = \hat{Y}_O = T - T_0 = 0$ in the fuel stream and $\hat{Y}_F = \hat{Y}_O - 1 = T - T_A = 0$ in the airstream. For noncatalytic walls, the condition of vanishing diffusion fluxes $\mathbf{n} \cdot \nabla \hat{Y}_F = \mathbf{n} \cdot \nabla \hat{Y}_O = 0$ must be imposed, with \mathbf{n} denoting the unit vector normal to the wall. Writing the boundary conditions for the temperature at the wall surface generally requires the solution of a conjugate heat conduction problem on the wall, with two limiting cases of practical

interest being that of isothermal walls, for which $T = T_w = \text{constant}$, and that of adiabatic walls, for which $\mathbf{n} \cdot \nabla T = 0$.

2.3. The Limit of Infinitely Fast Combustion

Two different physically relevant limits can be identified by considering the solution that emerges for extreme values of the frequency factor \hat{B} . In the limit $\hat{B} \rightarrow 0$, the reaction term vanishes in Equations 5–7, which then describe the frozen mixing between the fuel and air. Because of the small difference in molecular mass of O_2 and N_2 , when feeding with undiluted fuel, we can consider the mixture as binary, interdiffusing with the diffusivity D_F of the fuel, so that $\hat{Y}_\text{O} = 1 - \hat{Y}_F$ replaces Equation 6 in the computation of \hat{Y}_O .

In the opposite limit, $\hat{B} \rightarrow \infty$, the reaction takes place, at an infinitely fast rate, only in an infinitesimally thin layer Σ_f . On both the sides of the flame sheet, Σ_f , there is chemical equilibrium,

$$\hat{Y}_F \hat{Y}_\text{O} = 0, \quad (8)$$

with a region Ω_F in which $\hat{Y}_\text{O} = 0$ and a region Ω_O in which $\hat{Y}_F = 0$. The reaction-rate terms in Equations 5–7 then become Dirac delta distributions located at Σ_f , whose strengths satisfy the proportionality relations $[1, S, -\gamma(1 + S)]$. These Dirac delta distributions, sinks for the reactant and sources for the heat and products, are necessarily balanced in the conservation equations (Equations 5–7) by the diffusion terms, mainly by the changes in the diffusion flux normal to the flame. Therefore, they produce jumps at the flame sheet of these fluxes, satisfying the proportionality relations given above, and leading, for example, to the condition that the reactants must reach the flame in stoichiometric proportions. The solution to this free-boundary problem, involving the determination of the flame surface Σ_f , is difficult to handle in the numerical simulation of unsteady and turbulent flows when the flame is strongly corrugated and wrinkled.

The limit $\hat{B} \rightarrow \infty$ of infinitely fast chemical reaction was first addressed in the seminal work of Burke & Schumann (1928). By considering the case of equal diffusivities of the reactants, they showed how the intrinsic difficulties associated with the singular character of the solution can be circumvented by treating the oxygen as a “negative combustible gas” with equivalent mass fraction $-Y_{\text{O}_2}/s$, thereby reducing the problem to that of integrating a transport equation, with the flame determined by the surface of zero mass fraction of combustible gas. The method was used to calculate the flame surface for the particular case of equal parallel laminar streams of fuel and air. Shvab (1948) and Zel’dovich (1949) later generalized the procedure to describe nonpremixed diffusion-controlled combustion with $L_{\text{O}_2} = L_F = 1$. The needed extension to account for nonunity values of the Lewis numbers of the reactants is recent (Liñán 1991, 2001). As done in the earlier work (Shvab 1948, Zel’dovich 1949), we must start by eliminating the chemical terms by linear combinations of the conservation equations. Thus, multiplying Equation 5 by S and subtracting Equation 6 yield a chemistry-free conservation equation involving, for nonunity Lewis numbers, two linear scalar combinations of the mass fractions, i.e., the classical combination $S\hat{Y}_F - \hat{Y}_\text{O}$, appearing in the accumulation and convection terms, and a Lewis number-weighted combination $S\hat{Y}_F/L_F - \hat{Y}_\text{O}$, appearing in the diffusion terms, the latter being a conserved scalar in the fast reaction layer. It is convenient to normalize these coupling functions to be unity in the fuel stream and zero in the oxidizer stream, thereby giving the conservation equation

$$\frac{\partial}{\partial t}(\rho Z) + \nabla \cdot (\rho \mathbf{v} Z) - \nabla \cdot \left[\left(\frac{S/L_F + 1}{S + 1} \right) \rho D_T \nabla \tilde{Z} \right] = 0, \quad (9)$$

involving the two mixture-fraction variables

$$Z = \frac{S\hat{Y}_F - \hat{Y}_O + 1}{S + 1} \quad \text{and} \quad \tilde{Z} = \frac{S\hat{Y}_F/L_F - \hat{Y}_O + 1}{S/L_F + 1}. \quad (10)$$

Because the Lewis number of O_2 is assumed to be unity, we can eliminate the chemical term using a linear combination of Equations 6 and 7 to yield

$$\frac{\partial}{\partial t}(\rho H) + \nabla \cdot (\rho \mathbf{v} H - \rho D_T \nabla H) = -\frac{\nabla \cdot \mathbf{q}_R}{c_p T_A} \quad (11)$$

for the excess-enthalpy variable

$$H = \frac{T - T_A}{T_A} + \frac{\gamma(S + 1)}{S}(\hat{Y}_O - 1). \quad (12)$$

Equations 9 and 11 must be complemented with the chemical equilibrium condition given in Equation 8 and the definitions in Equations 10 and 12 to allow us to calculate \hat{Y}_F , \hat{Y}_O , and T in terms of Z (or \tilde{Z}) and H . Thus, we begin by noticing that the flame is located where \hat{Y}_F and \hat{Y}_O are simultaneously zero, corresponding to values of the mixture fraction $Z = Z_S = 1/(1 + S)$ and $\tilde{Z} = \tilde{Z}_S = 1/(1 + S/L_F)$. For $Z \geq Z_S$, we obtain

$$\hat{Y}_O = 0 \quad \text{and} \quad Y_F = \frac{Z - Z_S}{1 - Z_S} = \frac{\tilde{Z} - \tilde{Z}_S}{1 - \tilde{Z}_S}, \quad \frac{T - T_A}{T_A} = H + \frac{\gamma}{1 - Z_S}, \quad (13)$$

whereas for $Z \leq Z_S$, we obtain

$$Y_F = 0 \quad \text{and} \quad \hat{Y}_O = 1 - \frac{Z}{Z_S} = 1 - \frac{\tilde{Z}}{\tilde{Z}_S}, \quad \frac{T - T_A}{T_A} = H + \frac{\gamma}{1 - Z_S} \frac{Z}{Z_S}. \quad (14)$$

Equations 13 and 14 provide a relation, piecewise linear, between Z and \tilde{Z} , and also the mass fractions of reactants and the temperature in terms of the coupling functions everywhere in the flow field. Although one cannot expect the temperature and mass fractions to be discontinuous functions in the fast-reaction limit, their gradients will certainly have jumps at the flame sheet, whereas the gradients of the conserved scalars \tilde{Z} and H will be continuous at the flame. In contrast, the gradient of the classical mixture fraction Z jumps at the flame, corresponding to a localized chemical source.

Equations 9 and 11, together with the accompanying expressions in Equations 13 and 14, associated with the condition given in Equation 8 of the noncoexistence of the reactants, replace Equations 5–7 in the integration of the problem, thereby removing the singularity associated with the reaction term. The boundary conditions include $Z = \tilde{Z} = H = 0$ in the airstream and $Z - 1 = \tilde{Z} - 1 = H - H_F = 0$ in the fuel stream, where $H_F = (T_0 - T_A)/T_A - \gamma(S + 1)/S$. At the combustor walls, the condition of nonpermeability yields $\mathbf{n} \cdot \nabla \tilde{Z} = \mathbf{n} \cdot \nabla Z = 0$, whereas the boundary condition for H is generally more complicated, reducing to $\mathbf{n} \cdot \nabla H = 0$ for an adiabatic wall. If needed, source-free conservation equations, similar to Equation 9, that determine the product concentrations can be obtained from linear combinations accounting for nonunity Lewis numbers of CO_2 and H_2O . It is worth remarking that in both limiting cases $\hat{B} \rightarrow 0$ and $\hat{B} \rightarrow \infty$, the problem reduces to one of mixing, described in the last case in terms of conserved scalars unaffected by the chemical reactions. This mixing process is turbulent for the large Reynolds numbers typically found in applications (Dimotakis 2005), although with an important role played by the heat release of combustion.

The formulation presented above, used, for instance, by Liñán et al. (1994) and Carpio et al. (2012), simplifies to the classical Burke-Schumann analysis when $L_F = 1$, in which case $Z = \tilde{Z}$. Furthermore, for adiabatic walls and negligible effects of radiation, the solution for H can be seen

to reduce to $H/H_F = Z$, which can be used to show that the flame temperature T_f reduces in that case to $T_f = T_S$, with T_S given in Equation 2. In the more general case of $L_F \neq 1$, the flame temperature depends on the value of H at Σ_f , generally yielding a value that differs from the adiabatic flame value T_S , a noticeable effect of the differential diffusion of the fuel.

3. JET DIFFUSION FLAMES: CONTROLLING PARAMETERS AND LIMITING DESCRIPTIONS

Jet diffusion flames are ubiquitous in practical combustion systems. For instance, coaxial jet diffusion flames formed by injecting liquid oxygen into a high-speed, coaxial, hydrogen gas stream are found in rocket engines. The configuration shown in **Figure 1**, corresponding to a diluted fuel jet of radius a and injection velocity U_0 discharging into a coflowing airstream with velocity U_A , has been used widely in experimental and numerical investigations of nonpremixed combustion.

Aside from a factor ρ , the magnitudes of the different terms in Equations 5–7 are associated with the inverse of corresponding characteristic times, to be derived from the initial and boundary conditions. However, with the naive assumption $\hat{Y}_F \hat{Y}_O \sim 1$, the chemical terms in Equations 5–7 are seen to be given, in order of magnitude, by the inverse of the chemical time

$$t_{\text{ch}} = \{\hat{B} \exp[-E/(RT)]\}^{-1}, \quad (15)$$

a strongly dependent function of the local temperature. Using the scales a and U_0 of the jet problem provides the residence time a/U_0 for the convective term and the diffusion time a^2/D_T for the conduction and diffusion terms, when the gradients of mass fractions and dimensionless temperature T/T_A are of order $1/a$. This is the case for flows with order-unity values of the Péclet number, $Pe = 2U_0a/D_T$, which in gases is of the order of the Reynolds number, $Re = 2U_0a/\nu_0$, based on the kinematic diffusivity of the fuel stream ν_0 . In jet flames with pulsating fuel feed, the fuel-injection frequency characterizes the order of magnitude of the accumulation terms in Equations 5–7, whereas, with steady fuel feed, the residence time a/U_0 is also the time associated with the instabilities of the flow and serves to measure the local accumulation term.

If the Reynolds number is of order unity, the relative importance of the chemical reaction is measured by the ratio of the orders of magnitude of the reaction and convection terms, giving the Damköhler number,

$$Da = \left(\frac{E}{RT_S}\right)^3 \frac{a}{U_0} \frac{S_L^2}{D_T} \exp\left(-\frac{E}{RT_S} \frac{T_S - T}{T}\right), \quad (16)$$

which has been conveniently expressed by relating the frequency factor \hat{B} to the flame propagation velocity S_L for a stoichiometric mixture of air and undiluted fuel. According to the previous discussion, small values of the Damköhler number correspond to chemically frozen flows, in which the reactants mix without significant chemical reaction, whereas large values of Da yield chemical equilibrium solutions, in which the reactants can coexist only in a thin flame sheet separating the fuel and oxidizer domains.

Because of the typically large nondimensional activation energy $E/(RT_S) \gg 1$ of the reaction rate and the fairly strong exothermicity of the combustion reactions represented by the parameter γ in Equation 3, the Damköhler numbers Da_0 and Da_S evaluated at the higher of the two feed temperatures (e.g., T_0) and at the flame temperature T_S differ by many orders of magnitude. In most cases, one finds $Da_0 \ll 1 \ll Da_S$, under which conditions multiple solutions of the reactive mixing problem may exist, as explained below.

For nonhypergolic fuels, the initial Damköhler number Da_0 is negligibly small, so in the absence of an external ignition source, the mixing of the fuel jet with the surrounding air proceeds without

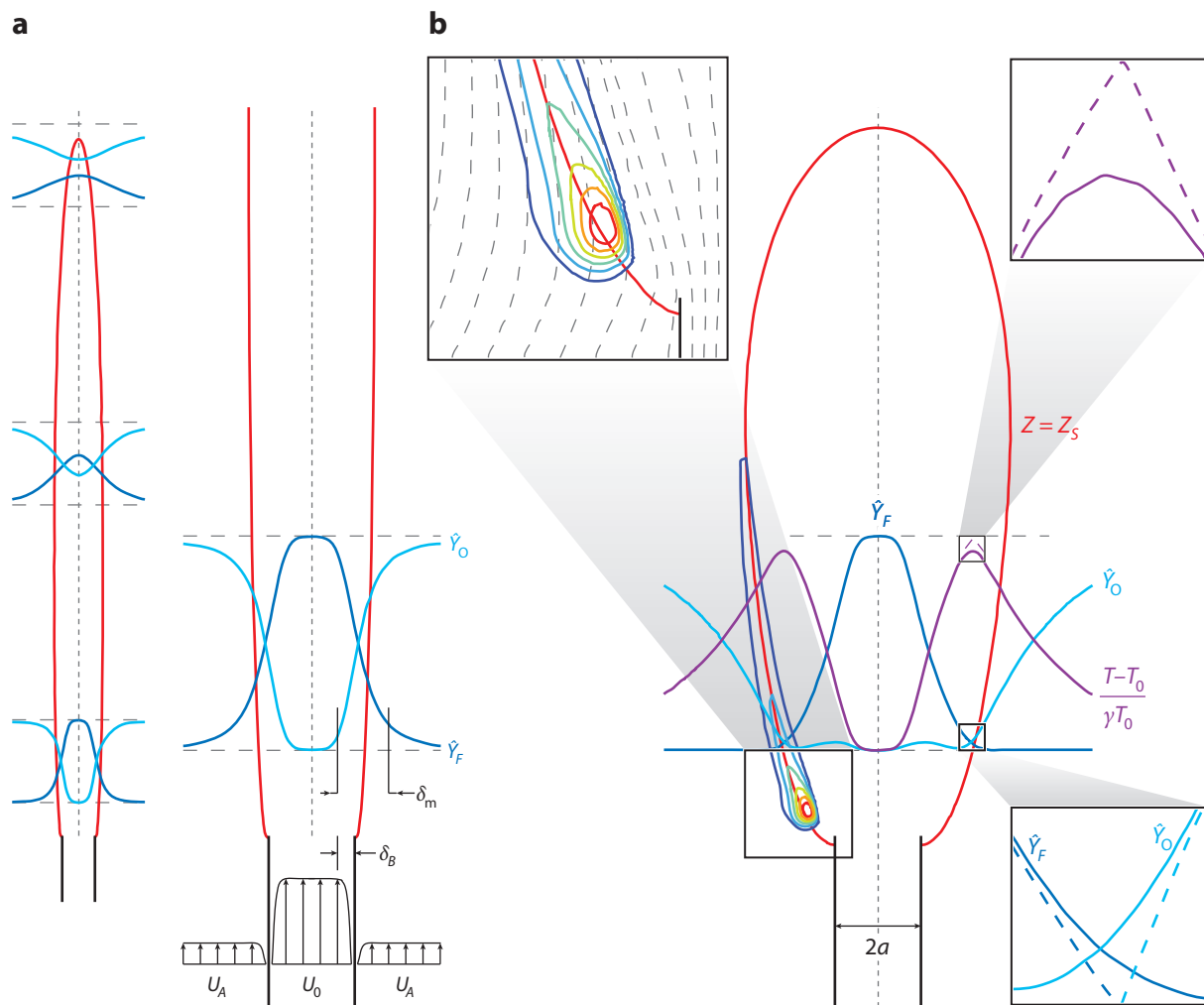


Figure 1

Diluted fuel jet with fuel mass fraction $Y_{F0} = 0.1$ and injection velocity U_0 discharging into a coflowing airstream with velocity $U_A = 0.1 U_0$ for $Re = 133$. Chemically frozen flow (a) and near-equilibrium jet diffusion flame (b) obtained with the flame sheet approximation and with the one-step Arrhenius chemistry model of Fernández-Tarrazo et al. (2006a). Figure courtesy of J. Carpio.

significant reaction. **Figure 1a** illustrates the chemically frozen jet flow, showing the surface $Z = Z_S = 1/(S + 1)$ at which the two reactants exist in stoichiometric proportions. Ignition can be forced externally by applying an ignition source (e.g., a spark or a hot body) at a point downstream from the injector where Z is close to Z_S , producing a local increase of the reaction rate that triggers the combustion process. The resulting premixed front, initially spherical, is immediately elongated by the flow, with the upstream part soon reaching a quasi-steady structure that propagates against the jet flow along the stoichiometric surface $Z = Z_S$. Depending on the flow conditions, this propagating flame may be blown off downstream; may propagate upstream and stabilize at a given location before reaching the injector, as a lifted flame; or may propagate

all the way upstream to anchor at the injector rim. We examine all these different aspects of the solution below, beginning with the structure and stability of attached jet diffusion flames.

4. THE STRUCTURE AND STABILITY OF DIFFUSION-CONTROLLED JET FLAMES

If $Da_S \gg 1$, then after ignition we may end up with a jet flame that is diffusion controlled everywhere outside a near-injector anchoring region, where the flame temperature drops well below T_S because of the heat loss to the injector wall. The flame-sheet approximation described in Section 2.3 can be used to compute the resulting flame, downstream from its small anchoring region (see, e.g., **Figure 1**, which also includes results obtained with finite-rate chemistry with a large value of Da). The flame-sheet shape given by $Z = Z_S$ is almost identical to that given by the reaction-rate contours of the finite-rate computation, except near the injector rim, at which the results with finite-rate kinetics clearly show the existence of an edge flame, obviously resulting from finite-rate effects. The oxygen that leaks to the interior of the jet in the anchoring region is clearly visible in the transverse profiles found one diameter downstream from the injector. The profiles also clearly show how the reactants coexist in the thin reaction layer when finite-rate chemistry is considered and that the sharp temperature profile of the Burke-Schumann solution is replaced by a rounded distribution with a smaller peak temperature.

The structure of jet diffusion flames depends fundamentally on the jet Reynolds number $Re = 2U_0a/v_0$. For the jet flame shown in **Figure 1**, the selected value $Re = 133$ is sufficiently large for the effect of diffusion to be limited initially to a thin annular mixing layer of characteristic thickness $\delta_m = (D_T x/U_0)^{1/2}$ separating the two streams, within which the diffusion time δ_m^2/D_T is comparable to the residence time. Across the mixing layer, the mixture fraction changes from $Z = 1$ on the fuel side to $Z = 0$ on the air side. The thickness δ_m increases to values of order a at distances of the order of the jet development length $L_d = Re a \gg a$. Downstream, the axial value of Z decreases as L_d/x . In the computation of **Figure 1**, the value of S is of order unity, resulting in a flame length that is of order L_d , although significantly shorter than the development length of the chemically frozen fuel jet, owing to the increase of D_T with temperature. For undiluted fuel feed, Z_S is very small, so the diffusion flame moves outward, reaching radial distances of order \sqrt{Sa} before closing on the axis at a distance $SL_d \gg L_d$.

For moderately large values of Re , the flow remains stable, and the boundary-layer approximation can be used to compute the resulting slender jet diffusion flame, as done earlier for vertical configurations (Li et al. 1995, Vázquez-Espí 2001), giving a solution that is independent of the Reynolds number. For $S \gg 1$, in the absence of coflow, the jet velocity has decreased at distances of the order of the flame length SL_d to values of order U_0/S , which must be compared with the buoyancy-induced velocity $\sqrt{gSL_d}$, so $U_0/(S^{3/2}\sqrt{g}L_d)$ emerges as the relevant Froude number. Simplified analyses of turbulent jet diffusion flames making use of the boundary-layer approximation together with a simple constant eddy-viscosity assumption for the turbulence modeling have had considerable success in predicting flame shapes (Peters & Göttgens 1991).

The description of diffusion flames at large Reynolds numbers is further complicated by the development of flow instabilities, which are clearly noticeable both in experiments and in numerical computations of jet diffusion flames (Chen & Roquemore 1986, Chen et al. 1988, Katta & Roquemore 1993, Roquemore & Katta 2000, Roquemore et al. 1989). **Figure 2** shows results of experimental visualizations (Chen et al. 1988) of a methane jet diffusion flame with $Re = 2,390$, along with numerical computations of the solution. The results help identify two different types of instabilities, each leading to qualitatively different vortical patterns. The small inner eddies are a result of the Kelvin-Helmholtz instability of the fuel jet, which develops into discrete coherent vortices

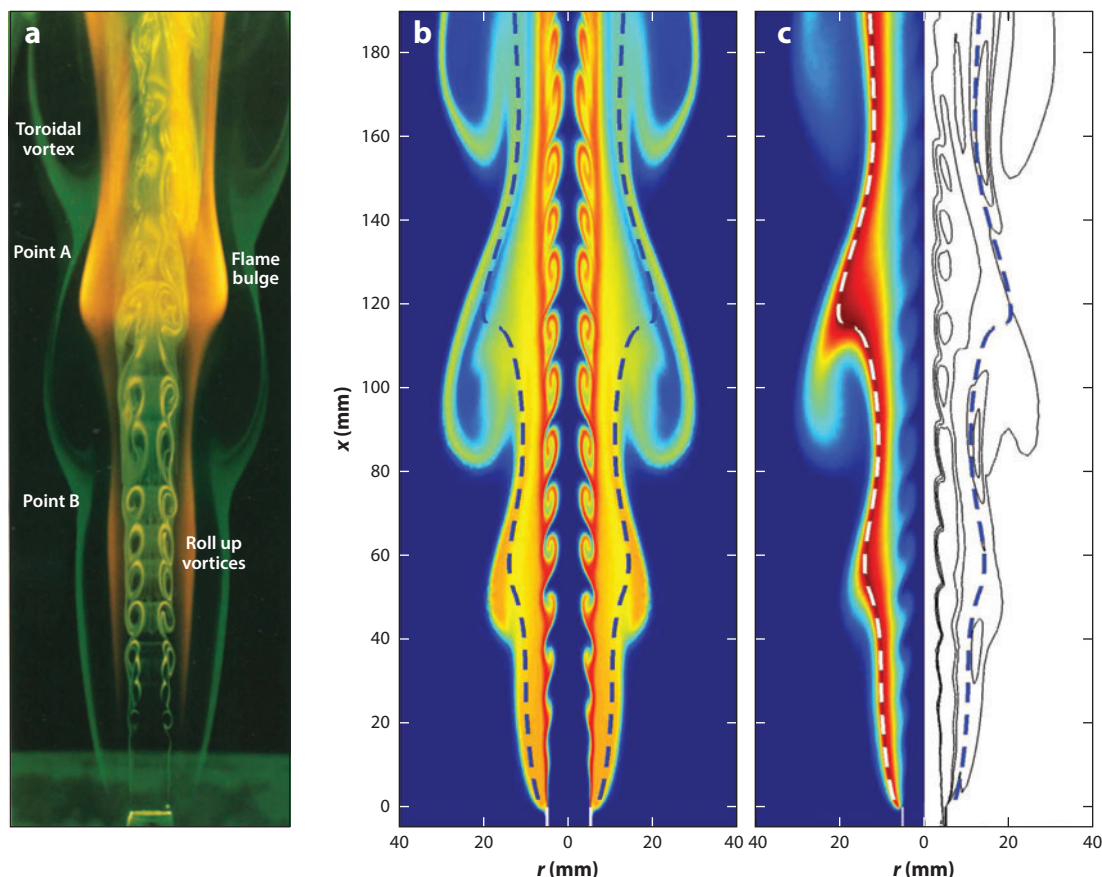


Figure 2

(a) Visualizations of a methane jet diffusion flame for $Re = 2,390$. Yellow represents light from the soot particles, bounded externally by the diffusion flame, and the green is Mie scattered laser light from the TiO_2 particles, marking the air/water and fuel/water product interfaces bounding the jet flame. Panel *a* adapted with permission from Chen et al. (1988) with replacement labeling, copyright Elsevier. (b,c) Numerical computations of the flow with a one-step Arrhenius chemistry model for the methane oxygen reaction (Fernández-Tarrazo et al. 2006a) and an infinitely fast approximation for the weakly exothermic reaction between $TiCl_4$ and water vapor. The integrations employ a finite-element numerical code (Carpio & Prieto 2014) previously used in other reactive jet computations (Carpio et al. 2013). Panel *b* shows concentration levels of TiO_2 , and panel *c* shows temperature and vorticity contours, with the flame marked in both plots by a dashed curve. Panels *b* and *c* courtesy of J. Carpio.

that grow in size by pairing. In **Figure 2**, the coherence persists as the jet develops downstream, resulting in an unsteady flow that remains transitional over a long distance (Roquemoire et al. 1989). There exists a critical value of Re , of the order of 4,000, above which three-dimensional instabilities appear close to the injector, generating a cascade of vortices of decreasing size in the mixing layer and triggering the so-called mixing transition (Dimotakis 2005) to a fully turbulent flow.

The large toroidal vortices surrounding the flame are of a different nature. They originate from an instability of the buoyant flow (Buckmaster & Peters 1986), responsible for the well-known phenomenon of diffusion-flame flickering (Chamberlin & Rose 1948). Numerical simulations (Jiang & Luo 2000) seem to indicate that this intrinsic flow instability is of an absolute unstable nature, giving rise to self-sustained oscillations that are independent of the flow perturbations. The resulting large vortices are seen to significantly affect the shape of the diffusion flame and may

even cause flame pinch-off when the amplitude of the associated oscillations becomes sufficiently large, leading to burning of individual fuel pockets (Carpio et al. 2012).

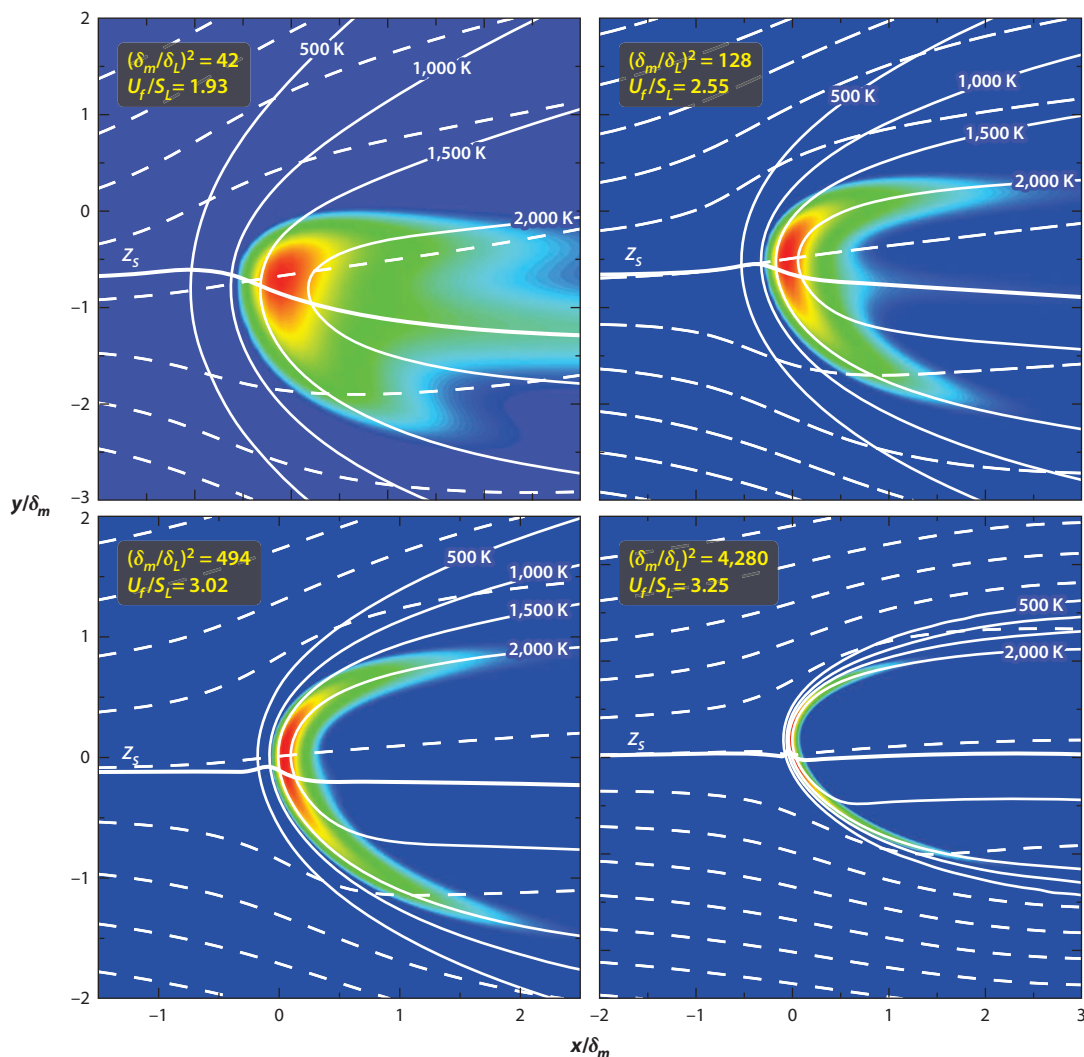
5. IGNITION, LIFTOFF, AND BLOW-OFF OF JET DIFFUSION FLAMES

Ignition of the frozen fuel jet can be achieved by locally applying a sufficiently energetic ignition source. For the large values of the Reynolds number typical of most practical applications, the flame front generated upon ignition is thin compared with the jet radius, and its local structure is that of a planar premixed flame, whose maximum propagation velocity S_L is reached when the mixture is nearly stoichiometric. Correspondingly, the premixed front that forms following ignition moves both upstream and downstream along the stoichiometric surface $Z = Z_S$ and exhibits a characteristic structure, first observed by Phillips (1965), including a lean branch and a rich branch (Kioni et al. 1993). On the lean side, the premixed flame consumes all the available fuel, leaving behind oxygen that reacts in a trailing diffusion flame with the fuel left behind by the rich branch. Because of the high sensitivity with temperature of the chemical reaction, measured by the Zel'dovich number, $\beta = E(T_S - T_0)/(RT_S^2) \gg 1$ (Williams 1985), the flame propagation velocity decays rapidly from S_L for either leaner or richer conditions. As a result, the lean and rich branches of the flame front curve backward from the leading stoichiometric point with a radius of curvature δ_m/β significantly smaller than the local mixing-layer thickness δ_m (Dold 1989, Dold et al. 1991), the latter related to the upstream concentration gradient at the stoichiometric surface according to $\delta_m \sim 1/|\nabla Z|_S$ or, more precisely, according to $\delta_m \sim Z_S/|\nabla Z|_S$, when $Z_S \ll 1$. The flame front loses its tribrachial structure as the value of the radius of curvature δ_m/β becomes comparable to the flame-front thickness $\delta_L = D_T/S_L$. The resulting flame structure is called a flame edge or an edge flame (Buckmaster 2002).

The triple flame moves relative to the flow with a propagation velocity, U_f , of the order of S_L . The flow in the nose region downstream from the flame is rotational, with overpressures that deflect outward the incoming streamlines and slow the flow velocity along the stoichiometric surface $Z = Z_S$. Correspondingly, the front propagation velocity, U_f , relative to the unperturbed flow, is larger than S_L by a factor of order $\gamma^{1/2}$ (Ruetsch et al. 1995). The value of U_f also depends on the transverse variation of the temperature, composition, and velocity ahead of the propagating flame, which are determined by the mixing process occurring upstream. For triple flames moving along locally planar mixing layers of thickness δ_m , this dependence is measured by the thickness ratio δ_m/δ_L or, equivalently, by the local Damköhler number $(\delta_m/\delta_L)^2$, defined as the ratio of the diffusion time across the mixing layer δ_m^2/D_T to the characteristic chemical time $\delta_L^2/D_T = D_T/S_L^2$.

Figure 3 shows results corresponding to triple flames propagating in isothermal, isovelocity, undiluted methane-air mixing layers for four different values of $(\delta_m/\delta_L)^2$ (Liñán et al. 2005). A one-step irreversible Arrhenius reaction with Zel'dovich number $\beta \simeq 6$ is used in the computations. Streamlines are plotted to exhibit the effect of the overpressure on the flow field. The values of the Damköhler numbers $(\delta_m/\delta_L)^2$ are selected to illustrate the evolution of the flame front from an edge flame for sufficiently small δ_m/δ_L to a thin premixed front with a negligibly weak trailing diffusion flame for $\delta_m/\delta_L \rightarrow \infty$. As can be seen, the transition occurs when the size of the flame-front region δ_m/β becomes comparable to δ_L , corresponding to a value of the more relevant Damköhler number $[\delta_m/(\beta\delta_L)]^2$ of order unity. We note that $\delta_m/(\beta\delta_L)$ also represents the ratio of the burning rate per unit flame surface in the premixed front and in the trailing diffusion flame, so for large values of the Damköhler number, the contributions of the burning rate in the diffusion flame cease to be visible.

The nondimensional propagation velocity U_f/S_L of the front relative to the upstream flow, also indicated in **Figure 3** for the different cases considered, is an increasing function of δ_m/δ_L


Figure 3

Two-dimensional methane-air edge flames propagating in isovelocity, isothermal ($T_0 = T_A = 300$ K) mixing layers. Solid curves indicate the isothermal (*thin*) and stoichiometric (*thick*) surfaces, and dashed curves are used for representative streamlines. Figure adapted with permission from Liñán et al. (2005).

that approaches an asymptotic value $U_f/S_L = 1.34\gamma^{1/2}$ for $\delta_m/\delta_L \rightarrow \infty$ (Fernández-Tarrazo et al. 2006b), leading to values of U_f exceeding $3S_L$ (Michaelis & Rogg 2005); for example, $U_f/S_L = 3.46$ when $\delta_m/\delta_L \rightarrow \infty$ for the conditions in **Figure 3**. This limiting value is associated with critical conditions for blow-off in planar mixing layers, a result in agreement with previous experimental observations (Muñiz & Mungal 1997).

The ignition, liftoff, and blow-off characteristics of jet diffusion flames depend fundamentally on the ability of the triple flame (or edge flame) to move upstream relative to the jet flow, so the ratio U_0/S_L becomes the key parameter in the description. The triple flame formed upon ignition will propagate all the way up to the injector for small values of U_0/S_L , whereas for values

of U_0/S_L of order unity, the flame will remain lifted, with a liftoff distance x_l that increases for increasing values of the jet velocity U_0 , or will be blown off when U_0/S_L exceeds a critical value. For moderately large values of Re , the solution depends on the thermochemical parameters S and γ , the Damköhler number $(a/\delta_L)^2$, the fuel Lewis number L_F , and the effects of buoyancy and coflow, measured by $U_0/\sqrt{gL_d}$ and U_A/U_0 (Liñán et al. 2005), with markedly different behaviors found in different regimes (Chung 2007).

Predictions of liftoff heights x_l can be obtained by equating the streamwise velocity $u_s(x)$ found along the stoichiometric surface $Z = Z_S$, which can be computed using the boundary-layer approximation when Re is moderately large (Revuelta et al. 2002), to the propagation velocity U_f , a procedure proposed by Lee & Chung (1997). For the resulting solution to be stable, the velocity difference $u_s - U_f$ must be a decreasing function of x at the liftoff location. When the lifted flame sits at a distance smaller than the jet development length $L_d = Re a$, the resulting triple flame is embedded in the annular mixing layer that surrounds the fuel jet, and its structure is locally two dimensional, similar to that of the flames shown in **Figure 3**. As a result, the corresponding value of U_f is an increasing function of x through its dependence on $\delta_m = (D_T x/U_0)^{1/2}$, thereby favoring the stability of the resulting lifted flame. The flame structure is no longer two dimensional for flames propagating at distances of order $L_d = Re a$ or larger, which may be encountered in undiluted configurations, for which the stoichiometric surface $Z = Z_S$ extends to large downstream distances $SL_d \gg L_d$. In this far-field region, the value of u_s , of order $u_s \sim U_0/S$ in the absence of coflow, can be calculated using the Schlichting-Squire solution to give $u_s \propto x^{(D_F/v-1)}$ (Lee & Chung 1997). As can be seen, the predicted value of u_s decreases with the downstream distance x when $D_F < v$, the case of heavy hydrocarbons, but it increases for $D_F > v$, a condition satisfied by methane and ethane. These different qualitative behaviors explain why lifted jet diffusion flames are more easily stabilized in experiments with undiluted fuel feed using propane and butane than they are when ethane and methane are employed (Lee & Chung 1997). For methane and ethane, the value of x determined by equating u_s and U_f corresponds to the furthest location at which one may generate a premixed front that propagates upstream to the injector rim by applying an ignition source.

Diffusion-flame ignition by triple-flame propagation cannot occur in high-speed combustion applications, for which the flow velocity is much larger than U_f . In those systems, the initial temperature of the reactants (typically the air in propulsion applications) is sufficiently high that the chemical reactions begin to occur as soon as the two reactants meet downstream from the injector rim, in a self-accelerating combustion process that leads to a spontaneous ignition event at a well-defined downstream location (Liñán & Crespo 1976).

6. THE ANCHORING REGION OF JET DIFFUSION FLAMES

The effects of upstream diffusion and conduction on the jet flow are negligibly small for $Re = 2U_0a/v_0 \gg 1$, except in a small NS region found near the rim of the injector, where the diffusion flame may be anchored (see **Figure 1**). As noted in early work (Gaydon & Wolfhard 1953), molecular mixing in this region creates a volume of combustible mixture that can sustain a diffusion flame edge propagating against the flow. The wall value of the fuel-stream velocity gradient A near the injector rim, determined by the thickness δ_B of the boundary layer that forms adjacent to the injector wall, enters in the scales of the anchoring region. In systems with coflowing air, a boundary layer also develops at the wall in the airstream, with the associated gradient α_A . As shown by Stewartson (1969) and Messiter (1970) in their analysis of the flow at the trailing edge of a splitter plate separating two parallel streams, when $\alpha \neq 0$ the flow near the injector rim exhibits a triple-deck structure, including nonnegligible spatial pressure variations that modify

the wall-velocity gradients, so the values A and α_A found at the end of the injector wall differ from those found upstream from the triple-deck region, of characteristic size $\delta_B Re^{1/8}$. The effects of heat release due to diffusion flames on the flow in the wake of injectors were analyzed by Higuera & Liñán (1996).

The characteristic size $\delta_N = \sqrt{v_0 A}$ and characteristic velocity $u_N = \sqrt{v_0 A}$ of the NS region, where the effects of upstream heat conduction and diffusion are significant, are determined by the condition $u_N \delta_N / v_0 = 1$. For the diffusion flame to remain attached to this NS region, one can anticipate that u_N should not significantly exceed S_L , or equivalently, the local Damköhler number $D_N = S_L^2 / (v_0 A)$ (the inverse of the relevant Karlovitz number $v_0 A / S_L^2$) should not be lower than a critical value $(D_N)_c$ of order unity.

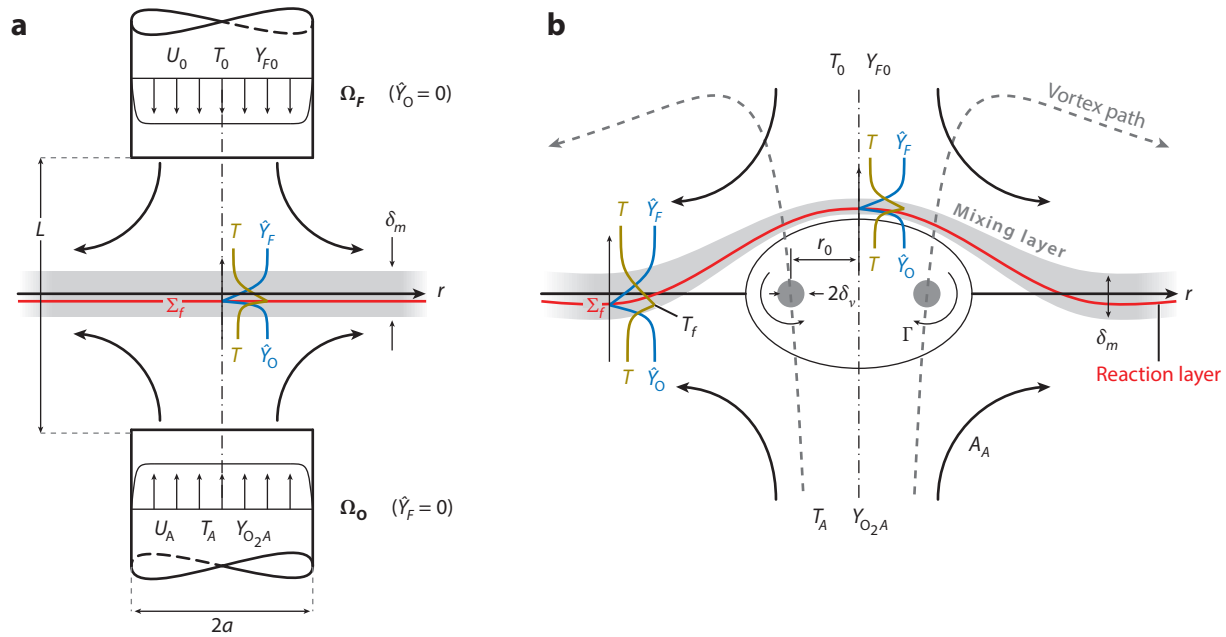
To calculate $(D_N)_c$, and the diffusion-flame edge structure for $D_N > (D_N)_c$, one must solve the locally two-dimensional and steady form of the reacting NS equations nondimensionalized with the scales δ_N and u_N (Fernández et al. 2000, Kurdyumov et al. 2002). With the scales of this NS region, the incoming air and fuel flows are seen as uniform shear flows at the temperature of the wall, intermediate between those of the two streams T_0 and T_A . The numerical integrations for decreasing values of D_N exhibit edge flames (Fernández et al. 2000, Kurdyumov et al. 2002) that separate progressively from the injector wall, giving overall heat-transfer rates to the wall that decrease rapidly as the value $(D_N)_c$ is approached. It is worth noting that the structure of the edge flames that form in the near wake of the injector is similar to that of the edge flames emerging in flame spread over solid fuels (Fernández-Tarrazo & Liñán 2002, Higuera 2002, Tizón et al. 1999).

When the Reynolds number based on the boundary-layer thickness $U_0 \delta_B / v_0$ exceeds a critical value, the boundary layer can be expected to become turbulent. In this case, the average values for the scales of the flame attachment region are the friction velocity and the thickness of the viscous sublayer, in which the local Reynolds number is of order unity and the Reynolds stresses are no longer dominant. The analysis of the attachment region can be anticipated to be similar to that of the laminar case, with the effect of turbulence introducing in this case time variations in the wall velocity gradients.

7. STRAIN-INDUCED EXTINCTION

Turbulent diffusion flames appear embedded in thin mixing layers that are locally distorted and strained by the turbulent motion. As shown by Liñán (1974), local flow extinction may occur for sufficiently large strain rates, when the rate of mixing (or, equivalently, the rate of fuel burning per unit flame surface), measured by $1/\delta_m \sim |\nabla Z|_S / Z_S$, is increased above a critical value, defined in order of magnitude by $1/\delta_m \sim 1/\delta_L \sim S_L / D_T$. These critical conditions correspond to values of the diffusion time across the mixing layer $\delta_m^2 / D_T \sim Z_S^2 / \chi_S$ of the order of the chemical time D_T / S_L^2 , with $\chi_S = D_T (\nabla Z)_S^2$ denoting the so-called scalar dissipation rate.

In the first approximation, the structure of the diffusion flames under near-extinction conditions is that corresponding to the infinitely fast reaction limit (Liñán 1974). Thus, the reaction zone lies in the stoichiometric surface $Z = Z_S$ and separates two regions of equilibrium flow. The inner structure is given by a diffusion-reaction balance, which was first analyzed in the limit $Da_S \gg 1$ by Liñán (1961, 1963) and Friedlander & Keller (1963), with higher-order terms incorporated in a subsequent analysis by Fendell (1965). As shown by Liñán (1974), to describe extinction, one needs to account for the strong temperature sensitivity of the reaction resulting from the large value of the activation energy, measured by the Zel'dovich number β . The analysis determines the critical value of the scalar dissipation rate at extinction, $(\chi_S)_e \sim Z_S^2 S_L^2 / D_T$ (see the **Supplemental Appendix**; follow the **Supplemental Material link** from the Annual Reviews home page at <http://www.annualreviews.org>).


Figure 4

(a) Schematic view of a steady counterflow diffusion flame. (b) Perturbations introduced by the head-on interaction with a laminar vortex ring introduced from the airstream.

In turbulent combustion applications, local flame extinction leads to the formation of flame holes (Nayagam et al. 1999, Pantano & Pullin 2003, Santoro et al. 2000b), which are separated by edge flames (Buckmaster 1996) from regions of near-equilibrium flow. Depending on the local value of the Damköhler number, $(\delta_m/\delta_L)^2$, these edge flames can propagate in either direction. That is, there exists a critical value of $(\delta_m/\delta_L)^2$ above which they propagate along the stoichiometric surface toward the unburned mixture as ignition fronts, whereas for smaller values of $(\delta_m/\delta_L)^2$, their propagation velocity relative to the incoming flow is negative, corresponding to failure waves that recede away from the unburned mixture (Cha & Ronney 2006, Daou & Liñán 1998, Shay & Ronney 1998).

A flow configuration of interest in connection with the high-Reynolds number flows typically encountered in burners is that of the counterflow mixing layer, which has been widely used as a canonical problem to represent local flow conditions in strained mixing layers (Peters 1986, 2000). The experimental arrangement employed to investigate counterflow diffusion flames involves two opposing nozzles separated a distance L (**Figure 4**). The resulting coaxial counterflowing jets, one of air and the other containing the gaseous fuel (often diluted with N_2), produce an axisymmetric laminar stagnation-point flow. For moderately large values of the Reynolds number, the flow of the counterflowing streams is nearly inviscid. Mixing between both streams occurs only in a thin layer located about the separating surface, whose characteristic thickness is $\delta_m \sim L/Re^{1/2} \ll L$. The structure of the thin mixing layer formed around the stagnation point, which exhibits a self-similar solution in terms of the distance z to the stagnation plane, depends on the strain rate exerted by the outer streams, of order U_A/L . Flame extinction is observed for values of the strain rate above a critical value $A_e \sim S_L^2/D_T \sim (\chi_s)_e$.

The head-on interaction of a vortex ring with a laminar counterflow diffusion flame constitutes a well-defined system, of intermediate complexity between steady laminar flames and turbulent ones. It is appropriate for the investigation of unsteady and curvature effects (Cuenot & Poinso 1994), as well as local flame extinction and reignition phenomena (Pantano & Pullin 2004), and has been widely used in the combustion community over the past two decades (Amantini et al. 2007, Katta et al. 1998, Renard et al. 2000, Rolon et al. 1995, Santoro et al. 2000a). Numerical and experimental studies of local flame extinction in nonpremixed flame-vortex interactions have led to the definition of the different interaction regimes in nonpremixed turbulent combustion diagrams, which summarize the current knowledge in the field (Peters 2000, Thévenin et al. 2000, Venugopal & Abraham 2008).

As sketched in **Figure 4**, this vortex-flame configuration can be characterized by the unperturbed strain experienced by the flame prior to the interaction, given by the value A_A on the air side of the mixing layer, the characteristic radius of the vortex ring r_0 , the vortex strength Γ , and a characteristic diffusivity of the system (e.g., the thermal diffusivity D_T or kinematic viscosity ν of the oxidizer stream) (Vera & Liñán 2004). Additional parameters include the temperature and composition of the fuel and oxidizer streams, which determine the critical strain rate at extinction A_c and the overall air-to-fuel mass stoichiometric ratio S .

Then, if we use A_A^{-1} and r_0 as time and length scales, three nondimensional parameters emerge, namely the nondimensional vortex strength, $\tilde{\Gamma} = A_\Gamma/A_A = \Gamma/(2A_A r_0^2)$, where $A_\Gamma = \Gamma/(2r_0^2)$ represents the characteristic strain imposed on the flame by the vortex; the Péclet number of the unperturbed flow, based on the characteristic size of the vortex r_0 , $Pe_0 = A_A r_0^2/D_T$; and the robustness of the flame, $\mathcal{R} = A_c/A_A$, which measures how far from extinction the flame is prior to the interaction with the vortex.

The above parameters are closely related to two alternative nondimensional numbers, namely the Reynolds number of the vortex based on the vortex circulation, $Re_\Gamma = \Gamma/\nu \sim \tilde{\Gamma} Pe_0$, and the vortex Damköhler number, $Da_\Gamma = A_c/A_\Gamma \sim \mathcal{R}/\tilde{\Gamma}$, defined as the ratio of the characteristic vortex turnover time, $1/A_\Gamma$, to the characteristic chemical time, $1/A_c$. Accordingly, local flame extinction should be expected for $Da_\Gamma \lesssim 1$.

Hermanns et al. (2007) used order-of-magnitude estimates to characterize the different regimes of diffusion flame-vortex interactions. These estimates led to various relations between the above nondimensional parameters that are suitable for inclusion in existing combustion diagrams, such as the extended diagram of interaction regimes shown in **Figure 5a**. As in Thévenin et al. (2000), the horizontal axis represents the ratio of the characteristic vortex size, $l_T \sim r_0$, to the characteristic laminar flame thickness, δ_L :

$$\frac{l_T}{\delta_L} \sim \frac{r_0}{D_T/S_L} = \frac{A_A r_0^2}{D_T} \frac{S_L}{A_A r_0} \sim (Pe_0 \mathcal{R})^{1/2}. \quad (17)$$

By contrast, the vertical axis represents the ratio of the characteristic vortex turnover velocity, $u_T \sim \Gamma/r_0$, to the planar stoichiometric flame velocity, S_L :

$$\frac{u_T}{S_L} \sim \frac{\Gamma/r_0}{S_L} = \frac{\Gamma}{A_A r_0^2} \frac{A_A r_0}{S_L} \sim \tilde{\Gamma} \left(\frac{Pe_0}{\mathcal{R}} \right)^{1/2}. \quad (18)$$

According to the above definitions, the diagonal dashed lines with slope -1 shown in **Figure 5a** correspond to constant values of the vortex Reynolds number, $Re_\Gamma \sim \tilde{\Gamma} Pe_0$, and the dashed lines with slope $+1$ correspond to constant values of the vortex Damköhler number, $Da_\Gamma \sim \tilde{\Gamma}/\mathcal{R}$. The diagram also shows the lines delimiting the different interaction regimes discussed in detail in Hermanns et al. (2007) and Vera et al. (2007).

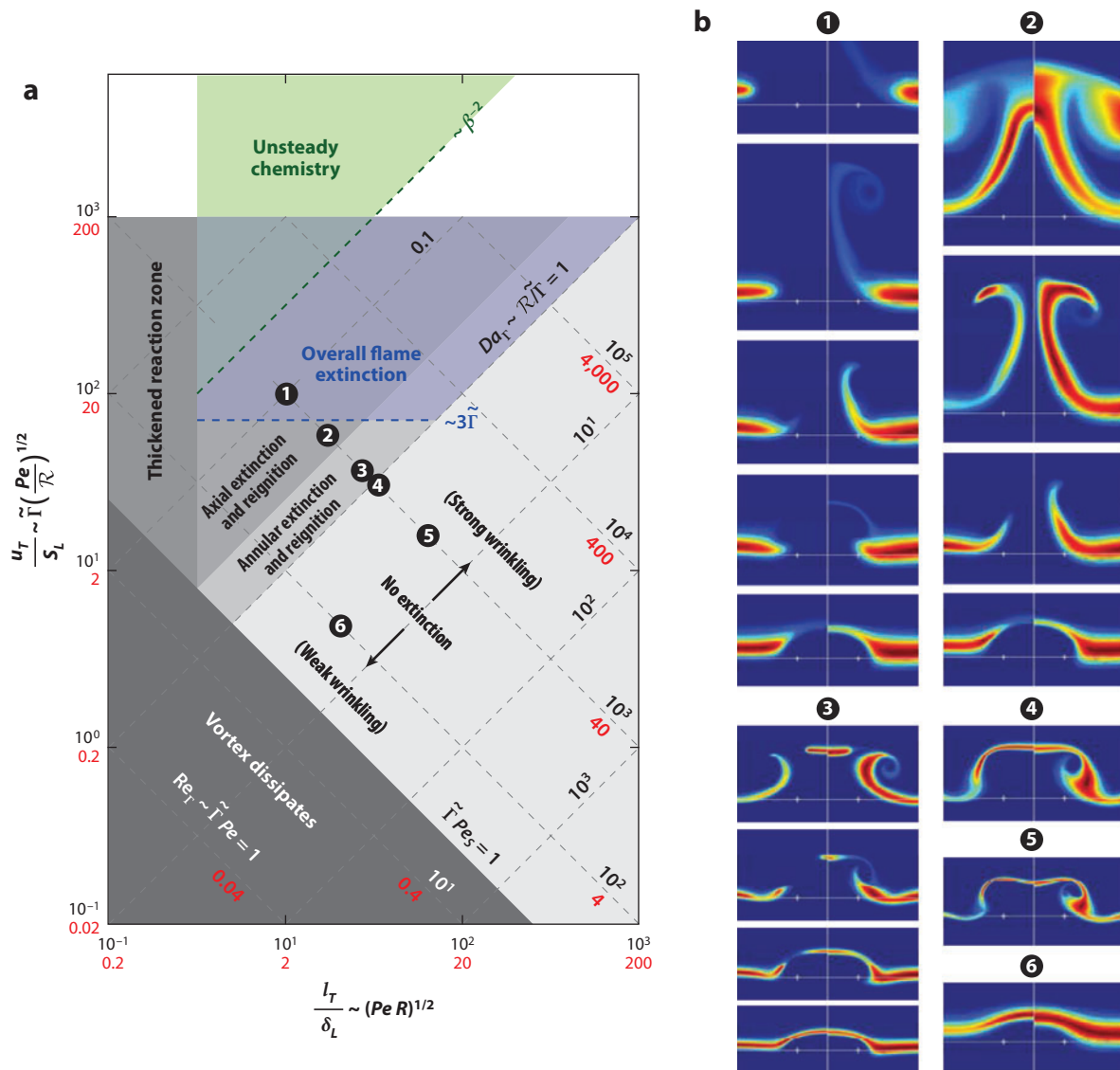


Figure 5

(a) Diagram of regimes of diffusion flame-vortex interactions in terms of the nondimensional vortex strength, $\tilde{\Gamma}$, the Péclet number of the unperturbed flow, Pe_A , and the robustness of the flame, \mathcal{R} . The horizontal and vertical axes represent the nondimensional size and velocity of the vortex, respectively. Values obtained using the diffusivity of air at the stoichiometric flame temperature are shown in red. (b) Illustrative simulations of diluted hydrogen-air diffusion flames interacting with laminar vortex rings are also shown, courtesy of J. Carpio. The values of the dimensionless parameters $(\tilde{\Gamma}, Pe_A, \mathcal{R})_i$ corresponding to point i are $(20, 50, 2)_1$, $(20, 50, 6)_2$, $(4.44, 225, 4)_3$, $(6, 167, 6)_4$, $(2, 500, 10)_5$, and $(2, 50, 10)_6$. Figure adapted with permission from Vera et al. (2007).

The variety of interaction regimes found in diffusion flame-vortex interactions is illustrated in **Figure 5b** by means of numerical simulations corresponding to diluted hydrogen-air diffusion (i.e., robust) flames interacting with sufficiently large and strong vortices. These include weakly distorted flames, strong flame wrinkling and roll up (followed often by flame pinch-off and pocket combustion), annular and axial extinction events followed by reignition via edge flames, and overall

flame extinction (Renard et al. 2000). We note that for less robust flames (e.g., methanol-air), most of the described phenomenology is not observed, and axial extinction prevails in most cases (Santoro & Gomez 2002).

8. CONCLUSIONS

We have aimed in this review to uncover the main parameters that control the existence, structure, ignition, and extinction of diffusion-controlled combustion of gaseous hydrocarbon fuels in air, using the jet diffusion flame as the main example. Some of the parameters are thermochemical, as the mass S of air needed to burn the unit mass of the fuel stream, and the nondimensional temperature rise γ when the mixture is burned at a constant pressure under homogeneous and adiabatic conditions. Other parameters are chemical kinetic, such as the flame propagation velocity S_L in the stoichiometric mixture defined above, and the nondimensional activation energy β that characterizes the strong dependence with the local temperature of the overall reaction rate. Other parameters are fluid dynamic, such as the Reynolds and Froude numbers of the jet flow and the Prandtl number and the Lewis numbers of the main species. We also call attention in this review to a generalization of the Burke-Schumann description of diffusion-controlled combustion to the realistic cases in which the Lewis numbers are nonunity.

DISCLOSURE STATEMENT

The authors are not aware of any biases that might be perceived as affecting the objectivity of this review.

ACKNOWLEDGMENTS

This work was supported by the Spanish MCINN through project CSD2010-00010. The authors are indebted to Dr. Jaime Carpio and Prof. Eduardo Fernández-Tarrazo for their assistance in the preparation of the figures.

LITERATURE CITED

- Amantini G, Frank JH, Bennett BAV, Smooke MD, Gomez A. 2007. Comprehensive study of the evolution of an annular edge flame during extinction and reignition of a counterflow diffusion flame perturbed by vortices. *Combust. Flame* 150:292–319
- Bilger RW. 1988. The structure of turbulent nonpremixed flames. *Proc. Combust. Inst.* 22:475–88
- Bilger RW, Pope SB, Bray KNC, Driscoll JF. 2005. Paradigms in turbulent combustion research. *Proc. Combust. Inst.* 30:21–42
- Buckmaster JD. 1996. Edge flames and their stability. *Combust. Sci. Technol.* 115:41–68
- Buckmaster JD. 2002. Edge-flames. *Prog. Energy Combust. Sci.* 28:435–75
- Buckmaster JD, Peters N. 1986. The infinite candle and its instability: a paradigm for flickering diffusion flames. *Proc. Combust. Inst.* 23:1829–36
- Burke SP, Schumann TEW. 1928. Diffusion flames. *Ind. Eng. Chem.* 20:998–1004
- Carpio J, Iglesias I, Vera M, Sánchez A, Liñán A. 2013. Critical radius for hot-jet ignition of hydrogen-air mixtures. *Int. J. Hydrog. Energy* 38:3105–9
- Carpio J, Prieto J. 2014. An anisotropic, fully adaptive algorithm for the solution of convection dominated equations with semi-Lagrangian schemes. *Comput. Methods Appl. Mech.* 273:77–99
- Carpio J, Sánchez-Sanz M, Fernández-Tarrazo E. 2012. Pinch-off in forced and non-forced, buoyant laminar jet diffusion flames. *Combust. Flame* 159:161–69

- Cha MS, Ronney PD. 2006. Propagation rates of nonpremixed edge flames. *Combust. Flame* 146:312–28
- Chamberlin DS, Rose A. 1948. The flicker of luminous flames. *Proc. Combust. Inst.* 1–2:27–32
- Chen LD, Roquemore WM. 1986. Visualization of jet flames. *Combust. Flame* 66:81–86
- Chen LD, Seaba JP, Roquemore WM, Goss LP. 1988. Buoyant diffusion flames. *Proc. Combust. Inst.* 22:677–84
- Chung SH. 2007. Stabilization, propagation and instability of tribrachial triple flames. *Proc. Combust. Inst.* 31:877–92
- Cuenot B, Poinot TJ. 1994. Effects of curvature and unsteadiness in diffusion flames: implications for turbulent diffusion flames. *Proc. Combust. Inst.* 25:1383–90
- Daou J, Liñán A. 1998. The role of unequal diffusivities in ignition and extinction fronts in strained mixing layers. *Combust. Theor. Model.* 2:449–77
- Dimotakis PE. 2005. Turbulent mixing. *Annu. Rev. Fluid Mech.* 37:329–56
- Dold JW. 1989. Flame propagation in a nonuniform mixture: analysis of a slowly varying triple flame. *Combust. Flame* 76:71–88
- Dold JW, Hartley LJ, Green D. 1991. Dynamics of laminar triple-flamelet structures in nonpremixed turbulent combustion. In *Dynamical Issues in Combustion Theory*, ed. PC Fife, A Liñán, FA Williams, pp. 83–106. New York: Springer
- Dowling AP, Morgans AS. 2005. Feedback control of combustion oscillations. *Annu. Rev. Fluid Mech.* 37:151–82
- Faraday M. 1861. *Chemical History of a Candle*. London: Griffin, Bohn & Co.
- Fendell FE. 1965. Ignition and extinction of initially unmixed reactants. *J. Fluid Mech.* 21:281–303
- Fernández E, Kurdyumov V, Liñán A. 2000. Diffusion flame attachment and lift-off in the near wake of a fuel injector. *Proc. Combust. Inst.* 28:2125–31
- Fernández-Tarrazo E, Liñán A. 2002. Flame spread over solid fuels in opposite natural convection. *Proc. Combust. Inst.* 29:219–25
- Fernández-Tarrazo E, Sánchez AL, Liñán A, Williams FA. 2006a. A simple one-step chemistry model for partially premixed hydrocarbon combustion. *Combust. Flame* 147:32–38
- Fernández-Tarrazo E, Vera M, Liñán A. 2006b. Liftoff and blowoff of a diffusion flame between parallel streams of fuel and air. *Combust. Flame* 144:261–76
- Friedlander SK, Keller KH. 1963. The structure of the zone of diffusion controlled combustion. *Chem. Eng. Sci.* 18:365–75
- Gaydon AG, Wolfhard HG. 1953. *Flames: Their Structure, Radiation, and Temperature*. London: Chapman & Hall
- Hermanns M, Vera M, Liñán A. 2007. On the dynamics of flame edges in diffusion-flame/vortex interactions. *Combust. Flame* 149:32–48
- Higuera FJ. 2002. Flame spread along horizontal solid fuel cylinders. *Proc. Combust. Inst.* 29:211–17
- Higuera FJ, Liñán A. 1996. Flow field of a diffusion flame attached to a thick-walled injector between two coflowing reactant streams. *J. Fluid Mech.* 329:389–411
- Jiang X, Luo KH. 2000. Combustion-induced buoyancy effects of an axisymmetric reactive plume. *Proc. Combust. Inst.* 28:1989–95
- Katta VR, Carter CD, Fiechtner GJ, Roquemore WM, Gord JR, Rolon JC. 1998. Interaction of a vortex with a flat flame formed between opposing jets of hydrogen and air. *Proc. Combust. Inst.* 27:587–94
- Katta VR, Roquemore WM. 1993. Role of inner and outer structures in transitional jet diffusion flame. *Combust. Flame* 93:274–82
- Kioni PN, Rogg B, Bray KNC, Liñán A. 1993. Flame spread in laminar mixing layers: the triple flame. *Combust. Flame* 95:276–90
- Kurdyumov V, Fernández-Tarrazo E, Liñán A. 2002. The anchoring of gaseous diffusion flames in stagnant air. *Aerosp. Sci. Technol.* 6:507–16
- Lee BJ, Chung SH. 1997. Stabilization of lifted tribrachial flames in a laminar nonpremixed jet. *Combust. Flame* 109:163–72
- Li SC, Gordon AS, Williams FA. 1995. A simplified method for the computation of Burke-Schumann flames in infinite atmospheres. *Combust. Sci. Technol.* 104:75–91
- Liñán A. 1961. *On the internal structure of laminar diffusion flames*. Tech. Rep. OSR/EOAR TN 62-24, INTA, Madrid

- Liñán A. 1963. *On the structure of laminar diffusion flames*. Aeronaut. Eng. Thesis, Calif. Inst. Technol., Pasadena
- Liñán A. 1974. The asymptotic structure of counterflow diffusion flames for large activation energies. *Acta Astronaut.* 1:1007–39
- Liñán A. 1991. The structure of diffusion flames. In *Fluid Dynamical Aspects of Combustion Theory*, ed. M Onofri, A Tesev, pp. 11–29. Harlow, UK: Longman Sci. Tech.
- Liñán A. 2001. Diffusion-controlled combustion. In *Mechanics for a New Millennium*, ed. H Aref, JW Phillips, pp. 487–502. Dordrecht: Kluwer Acad.
- Liñán A, Crespo A. 1976. An asymptotic analysis of unsteady diffusion flames for large activation energies. *Combust. Sci. Technol.* 14:95–117
- Liñán A, Fernández-Tarrazo E, Vera M, Sánchez AL. 2005. Lifted laminar jet diffusion flames. *Combust. Sci. Technol.* 177:933–53
- Liñán A, Orlandi P, Verzicco R, Higuera FJ. 1994. Effects of nonunity Lewis numbers on diffusion flames. In *Studying Turbulence Using Numerical Databases V*, pp. 5–18. Stanford, CA: Cent. Turbul. Res.
- Liñán A, Williams F. 1993. Ignition in an unsteady mixing layer subject to strain and variable pressure. *Combust. Flame* 95:31–46
- Liñán A, Williams F. 1995. Autoignition of nonuniform mixtures in chambers of variable volume. *Combust. Sci. Technol.* 105:245–63
- Libby P, Williams FA. 1994. *Turbulent Reacting Flows*. London: Academic
- Matalon M. 2007. Intrinsic flame instabilities in premixed and nonpremixed combustion. *Annu. Rev. Fluid Mech.* 39:163–91
- Messiter AF. 1970. Boundary-layer flow near the trailing edge of a flat plate. *SIAM J. Appl. Math.* 18:241–57
- Michaelis B, Rogg B. 2005. FEM-simulation of laminar flame propagation II: twin and triple flames in counterflow. *Combust. Sci. Technol.* 177:955–78
- Miller JA, Pilling MJ, Troe J. 2005. Unravelling combustion mechanisms through a quantitative understanding of elementary reactions. *Proc. Combust. Inst.* 30:43–88
- Muñiz L, Mungal MG. 1997. Instantaneous flame-stabilization velocities in lifted-jet diffusion flames. *Combust. Flame* 111:16–31
- Nayagam V, Balasubramaniam R, Ronney PD. 1999. Diffusion flame-holes. *Combust. Theor. Model.* 3:727–42
- Pantano C, Pullin DI. 2003. On the dynamics of the collapse of a diffusion-flame hole. *J. Fluid Mech.* 480:311–32
- Pantano C, Pullin DI. 2004. A statistical description of turbulent diffusion flame holes. *Combust. Flame* 137:295–305
- Peters N. 1984. Laminar diffusion flamelet models in non-premixed turbulent combustion. *Prog. Energy Combust. Sci.* 10:319–39
- Peters N. 1986. Laminar flamelet concepts in turbulent combustion. *Proc. Combust. Inst.* 21:1231–50
- Peters N. 2000. *Turbulent Combustion*. Cambridge, UK: Cambridge Univ. Press
- Peters N, Göttgens J. 1991. Scaling of buoyant turbulent jet diffusion flames. *Combust. Flame* 85:206–14
- Phillips H. 1965. Flame in a buoyant methane layer. *Proc. Combust. Inst.* 10:1277–83
- Pitsch H. 2006. Large-eddy simulation of turbulent combustion. *Annu. Rev. Fluid Mech.* 38:453–82
- Renard PH, Thévenin D, Rolon JC, Candel S. 2000. Dynamics of flame/vortex interactions. *Prog. Energy Combust. Sci.* 26:225–82
- Revuelta A, Sánchez AL, Liñán A. 2002. Laminar mixing in diluted and undiluted fuel jets upstream from lifted flames. *Combust. Flame* 128:199–210
- Rolon JC, Aguerre F, Candel S. 1995. Experiments on the interaction between a vortex and a strained diffusion flame. *Combust. Flame* 100:422–29
- Roquemore WM, Chen LD, Goss LP, Lynn WF. 1989. Structure of jet diffusion flames. In *Turbulent Reactive Flows*, ed. B Borghi, SNB Murthy, pp. 49–63. Berlin: Springer-Verlag
- Roquemore WM, Katta VR. 2000. Role of flow visualization in the development of UNICORN. *J. Vis.* 2:257–72
- Ruetsch GR, Vervish L, Liñán A. 1995. Effects of heat release on triple flames. *Phys. Fluids A* 7:1447–54
- Sánchez AL, Urzay J, Liñán A. 2015. The role of separation of scales in the description of spray flames. *Proc. Combust. Inst.* 35: In press

- Sánchez AL, Williams FA. 2014. Recent advances in understanding of flammability characteristics of hydrogen. *Prog. Energy Combust. Sci.* 41:1–55
- Santoro VS, Gomez A. 2002. Extinction and reignition in counterflow spray diffusion flames interacting with laminar vortices. *Proc. Combust. Inst.* 29:585–92
- Santoro VS, Kyritsis DC, Liñán A, Gomez A. 2000a. Vortex-induced extinction behavior in methanol gaseous flames: a comparison with quasi-steady extinction. *Proc. Combust. Inst.* 28:2109–16
- Santoro VS, Liñán A, Gomez A. 2000b. Propagation of edge flames in counterflow mixing layers: experiments and theory. *Proc. Combust. Inst.* 28:2039–46
- Shay ML, Ronney PD. 1998. Nonpremixed edge flames in spatially varying straining flows. *Combust. Flame* 112:171–80
- Shvab VA. 1948. The relationship between the temperature and velocity fields in a gaseous flame. In *Research on Combustion Processes in Natural Fuel*, ed. GF Knorre, pp. 231–48. Moscow: Gosenergoizdat
- Simmie JM. 2003. Detailed chemical kinetic models for the combustion of hydrocarbon fuels. *Prog. Energy Combust. Sci.* 29:599–634
- Sirignano WA. 2010. *Fluid Dynamics and Transport of Droplets and Sprays*. Cambridge, UK: Cambridge Univ. Press
- Stewartson K. 1969. On the flow near the trailing edge of a flat plate II. *Mathematika* 16:106–21
- Sunderland PB, Quintiere JG, Tabaka GA, Lian D, Chiu CW. 2011. Analysis and measurement of candle flame shapes. *Proc. Combust. Inst.* 33:2489–96
- Thévenin D, Renard PH, Fiechtner GJ, Gord JR, Rolon JC. 2000. Regimes of non-premixed flame-vortex interactions. *Proc. Combust. Inst.* 28:2101–8
- Tizón JM, Salvá JJ, Liñán A. 1999. Wind-aided flame spread under oblique forced flow. *Combust. Flame* 119:41–55
- Vázquez-Espí C. 2001. Analysis of axisymmetric laminar jet diffusion flames for small values of the stoichiometric mixture fraction. *Combust. Sci. Technol.* 171:1–38
- Venugopal R, Abraham J. 2008. A 2-D DNS investigation of extinction and reignition dynamics in non-premixed flame-vortex interactions. *Combust. Flame* 153:442–64
- Vera M, Hermanns M, Liñán A. 2007. A combustion diagram to characterize the regimes of interaction of non-premixed flames and strong vortices. *Proc. 3rd Eur. Combust. Meet. ECM 2007*. Crete: Greek Section Combust. Inst. http://www.combustion.org.uk/ECM_2007/ecm2007_papers/18-8.pdf
- Vera M, Liñán A. 2004. On the interaction of vortices with mixing layers. *Phys. Fluids* 16:2237–54
- Vervisch L, Poinso T. 1998. Direct numerical simulation of non-premixed turbulent flames. *Annu. Rev. Fluid Mech.* 30:655–91
- Veynante D, Vervisch L. 2002. Turbulent combustion modeling. *Prog. Energy Combust. Sci.* 28:193–266
- Westbrook CK, Dryer FL. 1981. Simplified reaction mechanisms for the oxidation of hydrocarbon fuels in flames. *Combust. Sci. Technol.* 27:31–43
- Williams FA. 1971. Theory of combustion in laminar flows. *Annu. Rev. Fluid Mech.* 3:171–88
- Williams FA. 1985. *Combustion Theory*. Menlo Park, CA: Benjamin Cummings. 2nd ed.
- Williams FA. 2000. Progress in knowledge of flamelet structure and extinction. *Prog. Energy Combust. Sci.* 26:657–82
- Zel'dovich YB. 1949. Teorii gorenia neperemeshannykh gazov. *Z. Tekh. Fiz.* 19:1199–1210